A class of upper-bound solutions for the extrusion of square shapes from square billets through curved dies

K.P. Maity*, P.K. Kar, N.S. Das

Department of Mechanical Engineering, Regional Engineering College, Rourkela, Orissa, India

Industrial summary

An upper-bound analysis is proposed for the extrusion of square sections from square billets through curved dies having prescribed profiles. Kinematically-admissible velocity fields for the purpose are derived using the dual-stream-function technique. Analytical results are presented for both frictionless and sticking friction conditions; for the latter situation the die geometry has been optimised with respect to appropriate parameters. It is shown that a cosine-shaped die with zero entry and exit angles yields the lowest extrusion pressure in the absence of friction, whilst the best upper-bound is provided by a straight tapered die under sticking-friction conditions. The internal work of deformation, however, is still found to be minimum for a straight die for frictionless extrusion.

Keywords: Extrusion; Square shapes; Square billets; Upper-bound analysis

1. Introduction

A number of analytical studies have been carried out during the past few years to compute the deformation loads for the extrusion/drawing of metals through curved dies. Such studies were initiated due to the use of these dies rendering the deformation more homogeneous with consequent reduction in the deformation load. Hence, for metals that are either difficult to form or where the temperature rise is to be minimized to protect the metallurgical structure of the deformed product, these dies can be used with advantage. The geometry of an ideal streamlined wire-drawing die of perfect efficiency was first proposed by Richmond and Devenpeck [1], the proposed die profile being sigmoidal with zero entry and exit angles, so that no tangential velocity discontinuities were introduced. Further, using slip-line-field analysis, it has been shown that for such dies the load is equal to that for homogeneous compression [2].

Slip-line-field solutions for some other die shapes have also been presented. Thus, for extrusion through cosine-shaped die, slip-line-field solutions were obtained by Samanta [3] and for parabolic-shaped dies by Bacharach and Samanta [4]. General upper-bound solutions for axi-symmetric extrusion through curved dies have been obtained by Chen and Ling [5] and Chang and Choi [6], with the foregoing analysis being used by Yang et al. [7] to determine the geometry of streamlined dies for axi-symmetric extrusion. Experimental results for extrusion through mathematically-contoured dies have also been presented by Frisch and Mata-Pietric [8,9].

Thus, it may be observed that for plane-strain and axi-symmetric extrusion through curved dies, adequate information is available in the literature. However, such information has not been reported to date for three-dimensional extrusion through mathematically-contoured dies.

In the present investigation, an attempt has been made to derive upper bounds for the extrusion of square sections from square billets using curved dies of prescribed profiles. The dies examined are cosine, elliptic, circular, parabolic and hyperbolic in shape, and kinematically-admissible velocity fields for all these cases have been obtained using the dual-stream-function method proposed by Nagpal and Altan [10]. Upper-bound extrusion loads for these dies are computed

for a number of reductions and for different friction conditions at the die-metal interface. It is observed that although a cosine-shaped die yields the least upper bound for frictionless extrusion, the internal work of deformation for this die is not necessarily the minimum. Further, for high friction conditions, the best results are still provided by a straight-tapered die.

2. Dual stream functions

For ideal fluid flow in three dimensions, Yih [11] suggested the use of two stream functions in place of one as in the case of a two-dimensional flow. Each stream function represents a class of surfaces called stream surfaces. The intersection line of two stream surfaces, one taken from each class, is a three-dimensional stream line.

Let $\varphi_1(x, y, z)$ and $\varphi_2(x, y, z)$ be two continuous functions satisfying the boundary conditions on velocity. These two functions, therefore, can be treated as a pair of dual stream functions. Following Yih [11], the velocity components can be derived from these stream functions using the equations:

$$V_x = (\partial\varphi_2/\partial y)(\partial\varphi_1/\partial z) - (\partial\varphi_1/\partial y)(\partial\varphi_2/\partial z) \tag{1a}$$

$$V_y = (\partial\varphi_2/\partial z)(\partial\varphi_1/\partial x) - (\partial\varphi_1/\partial z)(\partial\varphi_2/\partial x) \tag{1b}$$

$$V_z = (\partial\varphi_2/\partial x)(\partial\varphi_1/\partial y) - (\partial\varphi_1/\partial x)(\partial\varphi_2/\partial y) \tag{1c}$$

It can be verified easily that the velocity components determined in the above-mentioned manner identically satisfy the incompressibility condition:

$$(\partial V_x/\partial_x) + (\partial V_y/\partial y) + (\partial V_z/\partial z) = 0 \tag{2}$$

Thus, analysis of the flow field for any three-dimensional metal deformation problem reduces the determination of the corresponding dual stream functions satisfying the boundary conditions on velocity.

To derive the dual stream functions for the present problem, the geometry shown in Fig. 1(a) may be considered. Because of symmetry about two mutually-perpendicular axes, only one quadrant of the actual geometry needs to be considered, and this is shown in Fig. 1(b) along with the prescribed frame of reference.

Let $F(z)$ be the die-profile function such that the die faces in the x–z and y–z planes are represented by $x = F(z)$ and $y = F(z)$, respectively. The function $F(z)$ must satisfy the conditions that $F(z) = W$ at $z = 0$ and $F(z) = A$ at $x = L$, where W and A are the semi-widths of the billet and product, respectively, and L is the die length (Fig. 1). Further let the dual stream functions φ_1 and φ_2 be chosen as shown below:

$$\varphi_1 = x/F(z) \tag{4a}$$

$$\varphi_2 = W^2 V_b y/F(z) \tag{4b}$$

where V_b is the billet velocity. It can be verified easily that: (i) $\varphi_1 = 0$ on the plane $x = 0$ and $\varphi_1 = -1$ on the die surface $x = F(z)$; and (ii) $\varphi_2 = 0$ on the plane $y = 0$ and $\varphi_2 = W^2 V_b$ (which is a constant) on the die surface $y = F(z)$. Such constant values ensure that surfaces $x = 0$, $x = F(z)$, $y = 0$ and $y = F(z)$ are stream surfaces and, as such, velocity components normal to these surfaces vanish.

Thus, φ_1 and φ_2 defined in the above-mentioned manner satisfy all velocity boundary conditions. Hence, they are valid stream functions to generate a kinematically-admissible velocity field.

Substituting Eq. (4) into Eq. (1) and simplifying, the velocity components in the deformation region are:

$$V_x = W^2 V_b x F'/F^3 \tag{5a}$$

$$V_y = W^2 V_b y F'/F^3 \tag{5b}$$

$$V_z = W^2 V_b/F^2 \tag{5c}$$

where $F = F(z)$ and $F' = \mathrm{d}F/\mathrm{d}z$.

3. The upper-bound

The upper-bound theorem states that amongst all kinematically-admissible velocity fields the actual one minimises the expression:

$$J = (2\sigma_0/\sqrt{3})\int \sqrt{(\varepsilon_{ij}\varepsilon_{ij})}\,\mathrm{d}V + (\sigma_0/\sqrt{3})\int |\Delta V|_s\,\mathrm{d}S + (m\sigma_0/\sqrt{3})\int |\Delta V|_{sf}\,\mathrm{d}S_f \tag{6}$$

where J is the power dissipation rate, σ_0 is the flow stress, ε_{ij} is the derived strain-rate tensor, $|\Delta V|_s$ is the velocity discontinuity at the entry and exit surfaces, $|\Delta V|_{sf}$ is the velocity discontinuity at the die–metal interfaces S_f, and m is the friction factor.

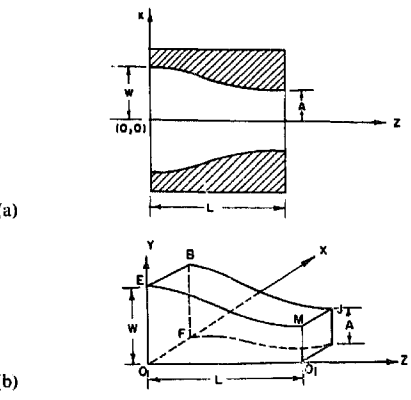

Fig. 1. Profile of a curved die with the axes of reference.

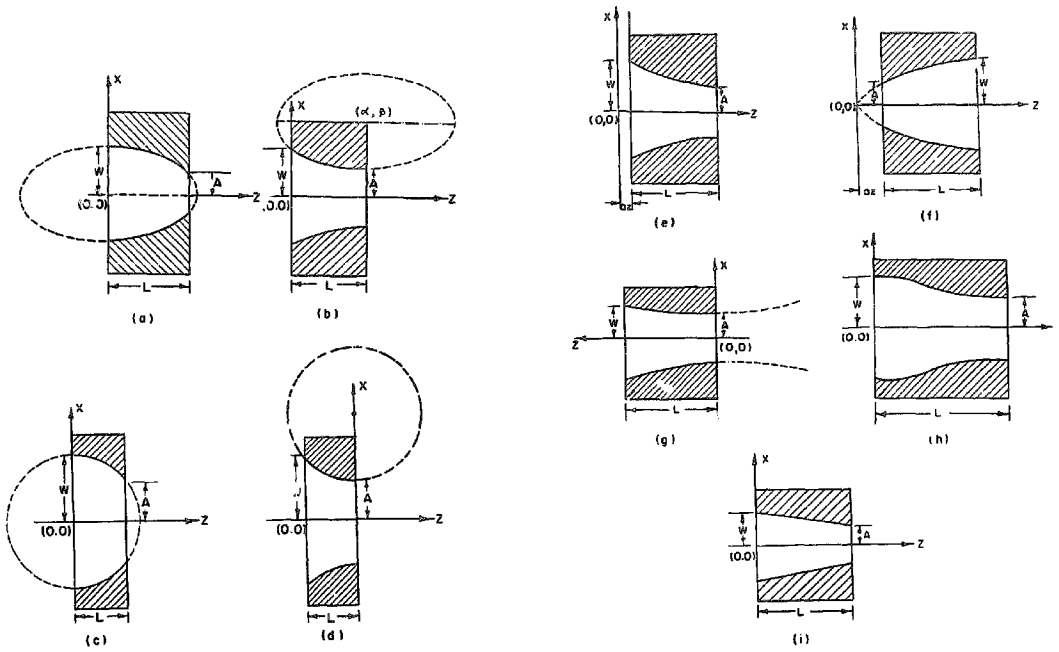

Fig. 2. Profiles of various curved dies with the axes of reference: (a) concave elliptical die; (b) convex elliptical die; (c) concave circular die; (d) convex circular die; (e) convex parabolic die; (f) concave parabolic die; (g) convex hyperbolic die; (h) cosine die, and (i) straight-tapered die.

The strain-rate components ε_{ij} are derived from the velocity components using the relationship:

$$\varepsilon_{ij} = (1/2)[(\partial V_i/\partial x_j) + (\partial V_j/\partial x_i)] \tag{7}$$

Substituting Eq. (5) into Eq. (7), the strain-rate components for the proposed flow field are written as:

$$\varepsilon_{xx} = (W^2 V_b F')/F^3$$

$$\varepsilon_{yy} = (W^2 V_b F')/F^3$$

$$\varepsilon_{zz} = (-2W^2 V_b F')/F^3$$

$$\varepsilon_{xy} = \varepsilon_{yx} = 0$$

$$\varepsilon_{yz} = \varepsilon_{zy} = (1/2) W^2 V_b y[(F''/F^3) - (3(F')^2/F^4)] \tag{8}$$

$$\varepsilon_{zx} = \varepsilon_{xz} = (1/2)\ W^2 V_b x[(F''/F^3) - (3(F')^2/F^4)]$$

where $F'' = d^2F/dz^2$. Using Eq. (8), J can be evaluated from Eq. (6) when the die-profile function, F, is known. For any reduction and friction factor m, J then can be minimized with respect to appropriate parameters to yield the best upper bound.

4. Die-profile function

The die geometries examined in the present investigation are shown in Fig. 2(a)–2(i), with the corresponding die-profile functions listed in Table 1. Referring to this Table, it may be seen that:

(a) the die-profile function $F(z)$ is similar in both the x- and y-directions;

(b) with the exception of the cosine-shaped die, the entry and exit angles are not simultaneously zero for the rest of the die shapes, and

(c) the velocity-discontinuity surfaces are straight in all cases.

5. Computation

An integrated Fortran code was developed to compute the upper-bound extrusion load using Eq. (6). For any given die-profile function, F, reduction, R, and friction factor, m, the program first calculates the velocity components and the strain-rate components using Eqs. (5) and (8), respectively, and then evaluates the upper-bound on power (Eq. (6)) by numerical integration using the 5-point Gauss–Legendre quadrature algorithm. The value of J obtained in the above-mentioned manner is then minimized with respect to appropriate parameters for any given configuration.

For convex elliptic and parabolic dies, there were two variable parameters (Table 1), the least upper-bound for these two cases was obtained using the Powell optimization algorithm [12]. For all other die shapes, the length L of the deformation zone was the only

optimizing parameter, the minimization for these cases was achieved through straight-forward calculation of J by varying L in small discrete steps. All the programs were implemented on a Vax-Vms mini-computer, and the time taken for each calculation was less than one second.

6. Results and discussion

The results from the present investigation are summarized in Figs. 3 and 4 for a smooth die ($m = 0$) and in Figs. 5 and 6 for a rough die ($m = 1.0$) for a number of reductions and for the different die profiles discussed in the text. The results reported in Figs. 3 and 4 are for an L/W ratio equal to 2.25 since, for the frictionless situation, no optimum die length was found to exist for any reduction. (The extrusion pressure decreased continuously with increase in length L of the deformation zone.)

Referring to Fig. 3, it may be seen that the least extrusion pressure is obtained for a cosine-shaped die having no velocity discontinuity at entry and exit, whilst a concave circular die yields the highest pressure. The internal work of deformation for any reduction for the latter is also found to be the maximum, as may be seen in Fig. 4. Further, the convex elliptic, circular and parabolic dies provide nearly similar results, with

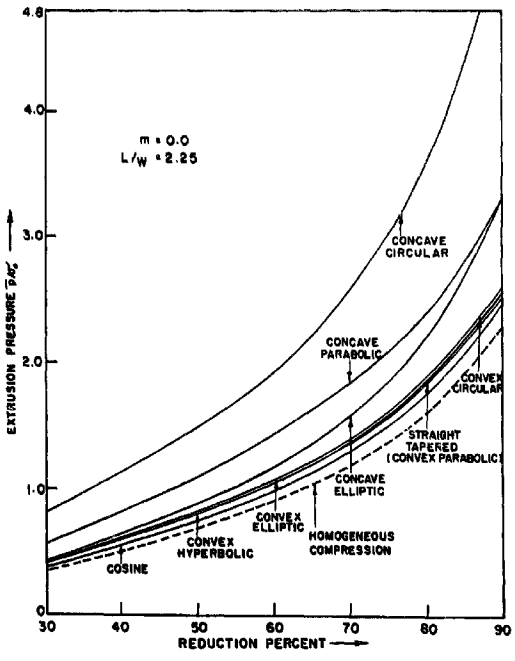

Fig. 3. Variation of the extrusion pressure with percentage reduction for smooth dies ($m = 0$).

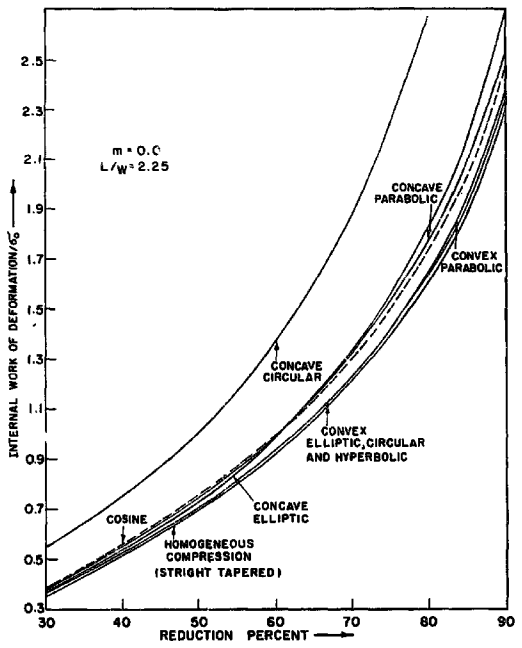

Fig. 4. Variation of the internal work of deformation with percentage reduction for smooth dies ($m = 0$).

slightly improved upper-bounds being obtained for a convex hyperbolic die (Fig. 3). The internal work of deformation for these dies is also of the same order and even lower than the corresponding values for a cosine-shaped die (Fig. 4). Thus, the inferior performance of this class of convex dies may be attributed to the expenditure of redundant work at entry (Table 1).

It appears, therefore, that it may be possible to design improved elliptic and hyperbolic dies having both concave and convex sections, to yield still lower extrusion pressure.

The variation of mean extrusion pressure with reduction in the case of the sticking friction condition ($m = 1.0$) for the above class of curved dies is shown in Fig. 5 and the corresponding variation of optimum die lengths is presented in Fig. 6. Referring to Fig. 5, it may be seen that the lowest upper bounds for this situation are provided by straight-tapered and convex parabolic dies with progressively increasing results obtained for cosine, convex hyperbolic, convex elliptic and convex circular profiles, in that order. The optimum die length for these different die shapes, however, is not found to follow any set pattern of variation with reduction, as may be seen in Fig. 6. Nevertheless, at low reductions the optimum die length for a convex parabolic die is found to be minimum, whilst the die length is minimum for a convex hyperbolic die at high reductions.

Table 1
Die geometries and die-profile functions

Die shape	Die-profile function, $F(z)$, $x = F(z)$, $y = F(Z)$	Entry angle	Exit angle	Remark
Concave elliptic	$[W^2-(W^2-A^2)(z/L)^2]^{0.5}$	0	$\neq 0$	Fig. 2(a)
Convex elliptic[a]	$\beta-b(1-((z-\alpha)/a)^2)^{0.5}$	$\neq 0$	0	Fig. 2(b)
Concave circular	$(W^2-z^2)^{0.5}$	0	$\neq 0$	Fig. 2(c)
Convex circular[b]	$\alpha-(R^2-(z-L)^2)^{0.5}$	$\neq 0$	0	Fig. 2(d)
Convex parabolic[c]	$W-(W-A)(\sqrt{az}-\sqrt{z})/[\sqrt{az}-\sqrt{(L+az)}]$	$\neq 0$	$\neq 0$	Fig. 2(e)
Concave parabolic[d]	$A+(W-A)(\sqrt{z}-\sqrt{az})/(\sqrt{(L+az)}-\sqrt{az})$	$\neq 0$	$\neq 0$	Fig. 2(f)
Convex hyperbolic	$(A^2+(W^2-A^2)(z/L)^2)^{0.5}$	$\neq 0$	0	Fig. 2(g)
Cosine	$(W+A)/2+((W-A)/2)\cos(\pi z/L)$	0	0	Fig. 2(h)
Straight-tapered	$A+(W-A)(L-z)/L$	$\neq 0$	$\neq 0$	Fig. 2(i)

[a] α, β are the coordinates of the centre of the ellipse: $\alpha = L$, $\beta = b+A$, $a = Lb/[(W-A)(2b-W+A)]^{0.5}$; a, b are the major and minor axes of the ellipse, respectively.
[b] α, β are the coordinates of the centre of the circle: R is the radius of the circle; $R = \beta - A$, $\beta = (A^2-W^2-L^2)/2(A-W)$.
[c] az is the distance between the x-axis and the entry plane.
[d] az is the distance between the x-axis and the exit plane.

It is interesting to note that a straight-tapered die with finite values of velocity discontinuity at entry and exit is not very inefficient in comparison to some of the curved dies analysed in the present study. Under low friction conditions this die compares favourable with a convex elliptic die (Fig. 3), whilst under high friction conditions it yields the lowest deformation load (Fig. 5). The internal work of deformation for this die is also found to be minimum (Fig. 4), as for any given reduction a straight-tapered die offers minimum surface area for interfacial friction and encloses the lowest deformation volume. A convex parabolic die is also found to yield results very close to those for a straight-tapered die, as the optimum die profile for this die is nearly straight. (The distance az between the apex of the parabola and the die entry is large (Fig. 2 (g).)

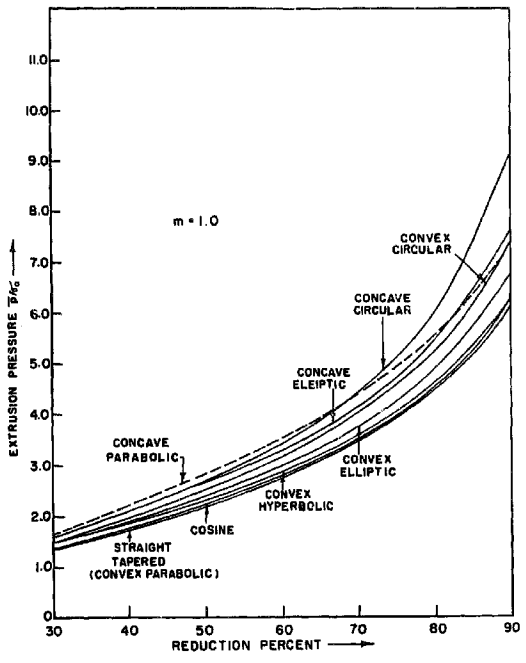

Fig. 5. Variation for the extrusion pressure with percentage reduction for dies with sticking friction ($m = 1$).

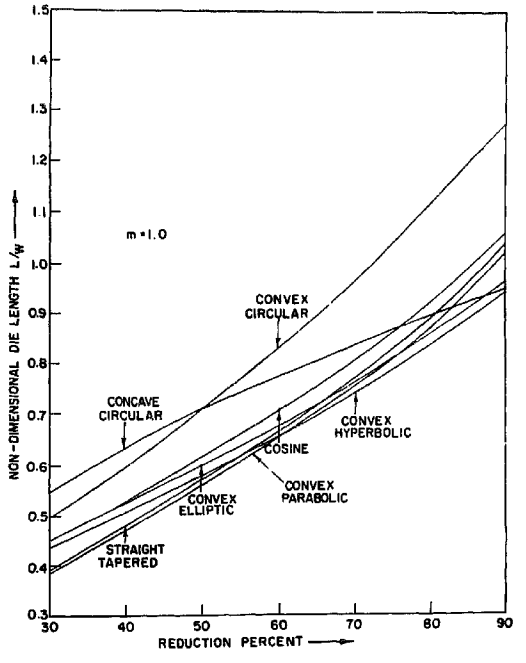

Fig. 6. Variation of the non-dimensional lengh with percentage reduction for dies with sticking friction ($m = 1$).

It may be mentioned here that the internal work of deformation for a straight-tapered die as computed from the dual-stream-function formulation is found to be close to that for homogeneous compression (Fig. 4). Thus, for this die, the deformation load calculated using Siebel's correction [13] may yield results similar to those obtained from the present analysis.

Referring to Figs. 3 and 5 it may be seen that concave dies yield higher deformation loads compared with the corresponding convex dies. This is because the deformation volume for a concave die is greater than that for a convex die for the same reduction.

7. Conclusions

Upper-bound loads for the extrusion of square sections from square billets have been computed using the dual-stream-function method for a number of concave and convex dies. It is seen that a cosine die yields the lowest extrusion pressure under frictionless conditions ($m = 0$), whilst under sticking-friction conditions ($m = 1.0$) a straight-tapered die provides the least pressure. The internal work of deformation is found to be minimum and nearly equal to that for homogeneous compression for a straight tapered die for $m = 0$. It is also seen that the upper bounds calculated for concave dies are always greater than those for convex dies, due to the greater deformation volumes enclosed by these latter dies.

8. List of symbols

A	half width of the product
F	$F(z)$ die profile function
F'	$F'(z)$ first derivative of F
F''	$F''(z)$ second derivative of F
J	upper-bound to power
L	die length
m	constant friction factor
p	average extrusion pressure
S	surface of the velocity discontinuity
S_f	friction surface
V_b	velocity of the billet
V_x, V_y, V_z	velocity components along the cartesian coordinate axes
W	half-width of the billet
$\lvert\Delta V\rvert_s$	magnitude of the velocity discontinuity at S
$\lvert\Delta V\rvert_{sf}$	magnitude of the velocity discontinuity at S_f

Greek letters

ε_{xx}, ε_{yy}, ε_{zz}	direct strain-rate components
ε_{xy}, ε_{yz}, ε_{zx}	shear strain-rate components
σ_0	uni-axial yield stress in compression
φ_1, φ_2	dual stream functions

References

[1] O. Richmond and M.L. Devenpeck, *Proc. 4th US Conf. Applied Mechanics*, American Society for Mechanical Engineers, New York, 1963, 1053.

[2] W. Johnson, R. Sowerby and J.B. Haddow, *Plane-strain Slip-line Fields, Theory and Bibliography*, E. Arnold, London, 1970.

[3] S.K. Samanta, Slip-line field for extrusion through cosine-shaped dies, *J. Mech. Phys., 18* (1973) 311.

[4] B.I. Bacharach and S. K. Samanta, *J. Appl. Mech., 43E* (1976) 97.

[5] C.T. Chen and F.F. Ling, *Int. J. Mech. Sci., 10* (1968) 863.

[6] K.T. Chang and J.C. Choi, *Proc. 12th Midwestern Mechanics Conf.*, University of Notre Dame, Paris, France, 1971.

[7] D.Y. Yang, C.H. Han and B.C. Lee, *Int. J. Mech. Sci., 27* (1985) 653-663.

[8] E. Mata-Pietri and J. Frisch, *Proc. North American Metal-Working Research Conf.*, Vol. 5, 1977.

[9] J. Frisch and E. Mata-Fietric, in J.M. Alexander (ed.), *Proc. 18th Int. Machine Tool Design Research Conf., London, Sept. 1977*, Macmillan, London, 1978, p. 55.

[10] V. Nagpal and T. Altan, *Proc. North American Metal for Research Conf., Pittsburgh, CA, USA*, Vol. 3, 1975, p. 26.

[11] C.S. Yih, *Stream Functions in Three-Dimensional Flow*, La Haulle Blanche, Vol. 12, 1957, p. 445.

[12] M.J.D. Powell, *Comput. J., 3* (1964).

[13] J.M. Alexander and R.C. Brewer, *Manufacturing Properties of Materials*, Van Nostrand Reinhold, New York, 1971.